Biosensors and Bioelectronics 55 (2014) 372–378

Contents lists available at ScienceDirect

Biosensors and Bioelectronics

journal homepage: www.elsevier.com/locate/bios

Synthesis and characterization of a stable, label-free optical biosensor from TiO_2-coated porous silicon

Jianlin Li [a,b], Michael J. Sailor [a,*]

[a] Department of Chemistry and Biochemistry, University of California, San Diego, La Jolla, California 92093, USA
[b] Gin College, Nanjing Normal University, Nanjing 210097, Jiangsu, China

ARTICLE INFO

Article history:
Received 12 September 2013
Received in revised form
17 November 2013
Accepted 4 December 2013
Available online 24 December 2013

Keywords:
Porous silicon
Chemical modification
Sol–gel chemistry
Label-free
Immunosensor

ABSTRACT

A nanoscale layer of TiO_2 is coated on the inner pore walls of a porous silicon (PSi) film by room-temperature infiltration of a TiO_2 sol–gel precursor and firing at 500 °C. The PSi:TiO_2 composite films are characterized by Fourier transform infrared (FTIR), X-ray diffraction (XRD), energy dispersive X-ray spectral analysis (EDS), scanning electron microscopy (SEM) and reflective interferometric Fourier transform spectroscopy (RIFTS). The analysis indicates that TiO_2 conformally coats the inner pore surfaces of the PSi film. The film displays greater aqueous stability in the pH range 2–12 relative to a PSi:SiO_2 surface. A label-free optical interference immunosensor based on the TiO_2-coated PSi film is demonstrated by real-time monitoring of the physical adsorption of protein A, followed by the specific binding of rabbit anti-sheep immunoglobulin (IgG) and then specific capture of sheep IgG. The time to achieve equilibrium for the physical adsorption of protein A on the surface of TiO_2-coated PSi film is significantly greater than that of PSi film. The specificity of the protein A and rabbit anti-sheep IgG construct on the sensor is confirmed by tests with non-binding chicken IgG. The sensitivity of the immunosensor is shown to be 8210 ± 170 nm/refractive index unit (RIU).

1. Introduction

Sensitive and stable label-free biosensors are desired for biological detection, environmental monitoring, drug development and food safety applications (Alvarez et al., 2009; Bonanno et al., 2010; Mun et al., 2010; Ouyang et al., 2005). Label-free biosensors combine the advantages of simplicity of sample preparation with ease of integration into high-throughput arrays. Transducers for optical label-free biosensors include surface plasmon resonance (SPR; Bolduc et al., 2010; Dupont et al., 2011), thin-film interference (Alvarez et al., 2009; Bonanno et al., 2010; Mun et al., 2010; Orosco et al., 2009; Ouyang et al., 2005) and optical waveguide (Cadarso et al., 2008) technologies. The reflective interferometric Fourier-transform spectroscopy (RIFTS) technique based on porous silicon (PSi) thin films has been shown to provide a sensitive, effective and simple means for achieving label-free optical biosensing (Bonanno et al., 2010; Jane et al., 2009; Meskini et al., 2007; Mun et al., 2010; Orosco et al., 2009; Ouyang et al., 2005;Schwartz et al., 2007a, 2007b). When the target analyte, such as complementary DNA, antibody (antigen), or aptamer, binds to its corresponding capture probe immobilized on the sensing substrate, a change in the average refractive index of the thin film is detected as a shift in wavelength of the characteristic spectral peak (Sailor, 2007).

PSi biosensors have been widely used as a detection platform for biomolecules because of their unique physicochemical properties (Bonanno et al., 2010; Orosco et al., 2009): (1) PSi is easily fabricated; (2) high-fidelity optical nanostructures such as rugate filters, multilayers, and Bragg stacks can be prepared that improve sensitivity of the optical measurement; (3) the surface of PSi is easy to chemically modify; and (4) PSi is compatible with microelectronics and MEMS fabrication systems. However, a particular challenge for PSi biosensors has been their chemical stability (Alvarez et al., 2009; Dancil et al., 1999; Mun et al., 2010). As-prepared hydride-terminated PSi is oxidized rapidly in the presence of oxygen and water, which results in degradation of the surface and zero point drift in the optical response of the sensor (Bocking et al., 2008; Boukherroub et al., 2001; Gurtner et al., 1999; Lees et al., 2003; Pacholski et al., 2005, 2006). To solve this problem, two main chemical stabilization methods have been used. One is through thermal oxidation to form Si–O bonds (Dancil et al., 1999; Delouise et al., 2004; Van Noort et al., 1998). However, the oxidized PSi surface is not particularly stable in biological media because it is susceptible to nucleophilic attack (Sailor, 2007). The second main approach has been the formation of covalent Si–C-bound organic monolayers by addition of Grignard, alkyllithium, or hydrosilylation reagents (Buriak, 2002; Guan et al., 2010; Gurtner et al., 1999; Linford and Chidsey, 1993).

* Corresponding author.
E-mail address: msailor@ucsd.edu (M.J. Sailor).

0956-5663/$ - see front matter © 2013 Elsevier B.V. All rights reserved.
http://dx.doi.org/10.1016/j.bios.2013.12.016

Although Si–C-bound organic monolayers are more stable, the surfaces are still subject to various degrees of corrosion and dissolution under physiological or higher pH conditions (Mun et al., 2010). Alternative porous optical materials such as TiO_2 nanotube arrays (Mun et al., 2010) have shown improved stability and in some cases greater sensitivity (Mun et al., 2010), and composites consisting of PSi and carbon have recently shown excellent stability (Sciacca et al., 2010), even in aggressive aqueous media (Tsang et al., 2012). The porous Si system allows somewhat greater control over nanostructure than TiO_2, including the construction of complex photonic crystals and the control of pore size.

Another challenge in porous optical biosensor devices is accumulation of impurities nonspecifically bound to the sensor surface, which leads to zero point drift and degradation of sensitivity. Sensors made from porous TiO_2 films (Li et al., 2008), nanotube arrays (Chen et al., 2010; Mun et al., 2010; Song and Schmuki, 2010), or 3D photonic crystals (Li et al., 2008, 2009; Wei, et al., 2011) are attractive in this regard, because the photoresponse of this high-bandgap semiconductor can be used to photocatalytically oxidize and refresh the sensor surface (Li et al., 2008; Liang et al., 2012). Titania is also of interest for in vivo sensing applications due to its biocompatibility (Kang et al., 2010).

The porous TiO_2 sensing substrate is not only more stable than PSi and alumina (Al_2O_3) substrates, but also more sensitive than PSi because of its larger refractive index ($n=2.5$; Alvarez et al., 2009; Mun et al., 2010). In this work we were interested in determining if the greater stability of TiO_2 could be incorporated into the more readily fabricated optical nanostructure of a PSi substrate, by modifying the inner pore surfaces of a PSi layer with TiO_2 sol–gel. We found the TiO_2 -coated PSi biosensor to be more stable under a wide range of pH values, and with sensitivity on the same order of magnitude as other PSi-based optical biosensors for real-time detection of protein adsorption and immunosensing.

2. Experimental section

2.1. Materials

Buffer solutions (pH 2–12) were obtained from VWR BDH. Phosphate buffer saline (PBS,1 × Cellgro brand, pH 7.4) was obtained from Mediatech, Inc. Protein A (42 kDa) from *Staphylococcus aureus* was purchased from EMD Calbiochem. Rabbit anti-sheep IgG, sheep IgG and chicken IgG were obtained from Jackson Immuno Research Laboratories, Inc. Silicon wafers (0.0008–0.0012 Ω cm resistivity, polished on the (1 0 0) face, B-doped) were obtained from Siltronix Corp. Other chemicals were purchased from Sigma-Aldrich Chemicals.

2.2. Preparation of porous silicon (PSi)

PSi samples were prepared by anodically etching highly doped p^{++}-type silicon using a Teflon etch cell and a platinum counter-electrode as previously described (Sailor, 2012). The electrolyte consisted of a 3:1 (v:v) mixture of aqueous 48% HF and absolute ethanol. The wafer was first cleaned by etching a sacrificial layer of porous Si at a current density of 106 mA/cm^2 for 30 s in dark. The anodized layer was then removed by treatment with an aqueous solution of NaOH (1 M) for ~1 min. The resulting shiny flat silicon surface was rinsed with ethanol, dried under a stream of nitrogen, and then the HF electrolyte was added to the etch cell. The sample was anodized at a current density of 620 mA/cm^2 for 20 s in dark, rinsed with absolute ethanol and then dried under a stream of nitrogen. The resulting PSi sample was oxidized in flowing ozone gas (9.8×10^{-2} m^3/h) for 20 min.

2.3. Preparation of TiO_2-coated PSi

A TiO_2 sol–gel precursor was prepared from a solution of 5:30:1 titanium butoxide:ethanol:triethanolamine (v/v) by rapid mixing with a vortex mixer in a sealed tube for 10 min. The TiO_2 sol–gel precursor (100 μL) was deposited on the PSi surface by spin coating (2000 rpm). The infiltrated sample was then heated in a tube furnace (in air) at 500 °C for 1 h. The deposition process was repeated three times on each sample.

2.4. Preparation of thermally oxidized porous Si ($PSiO_2$)

To prepare the fully oxidized $PSiO_2$ specimens, the freshly etched PSi sample was heated at 700 °C for 1 h in ambient air.

2.5. Interferometeric reflectance spectra

Reflectance spectra were acquired using an Ocean Optics USB-2000 CCD spectrometer fitted to a bifurcated fiber optic cable. The distal end of the combined fiber was attached to a microscope objective lens for allowing acquisition of 180° reflectance spectra from the sample surface, with a spot size of approximately 1–2 mm^2.

2.6. Characterization of TiO_2-coated PSi

Scanning electron microscope (SEM) images and energy dispersed X-ray spectra (EDS) were obtained with a FEI XL30 microscope equipped with a field emission gun and through-the-lens detector at an accelerating voltage of 5 kV. The optical thickness (nL) and porosity of samples were determined using the spectroscopic liquid infiltration method (SLIM), which involved analysis of the reflectance spectra of the film obtained in air and infiltrated with absolute ethanol, as previously described (Alvarez et al., 2009; Mun et al., 2010; Segal et al., 2007). X-ray diffraction (XRD) data were obtained using a Rigaku D/max 2550 VB/PC diffractometer with monochromated copper radiation at a scanning rate of 0.02°/s for values of 2θ ranging from 20° to 80°. Fourier transform infrared (FTIR) spectra were obtained with a Nicolet 6700 spectrometer (Thermo Scientific).

2.7. Stability of TiO_2-coated PSi

Aqueous stability tests of the TiO_2-coated PSi and $PSiO_2$ samples were performed as described previously (Mun et al., 2010). Briefly, the sample was mounted in a transparent poly (methyl) methacrylate flow cell (Supplemental Fig. S1) and buffer solutions in the pH range 2–12 were delivered by a peristaltic pump at a flow rate of 0.7 mL/min at room temperature. The optical reflectance spectrum was monitored through a transparent window in the flow cell for real-time (acquisition every 6 s), which allowed determination of optical thickness as a function of time. A baseline was acquired using pH 7.4 PBS solution, and then buffer solutions of the desired pH were introduced sequentially. The flow cell was rinsed with the pH 7.4 PBS solution between introductions of each buffer solution.

2.8. TiO_2-coated PSi immunosensor experiments

The immunosensor experiments were carried out in the same flow cell as in the above experiments. The sample in the flow cell was first rinsed with deionized water for 15–20 min and then flowing pH 7.4 PBS solution was introduced for a period of time sufficient to obtain a constant steady-state value of optical thickness. Solutions of the test proteins, protein A, rabbit anti-sheep IgG, and sheep IgG (3 mL, 0.1 mg/mL each), were then introduced

at a flow rate of 0.7 mL/min and continuously circulated until a steady-state value of optical thickness was obtained. The flow cell was then rinsed with pH 7.4 PBS to achieve a final steady-state value of optical thickness, typically within 5 min.

2.9. Sensitivity experiments

The TiO_2-coated PSi and $PSiO_2$ samples were immersed in organic liquids with different refractive indexes and the optical thickness values were determined from the interferometric reflectance spectrum. After each measurement, the sample was rinsed with absolute ethanol and dried in a stream of nitrogen.

3. Results and discussion

3.1. Synthesis and characterization of TiO_2-coated PSi films

The procedure used to prepare the TiO_2-coated PSi samples involves three steps in Scheme 1. An as-etched PSi film is first oxidized under a stream of ozone. This oxidative treatment generates a thin, hydrophilic silanol layer on the pore walls (Sailor, 2012). A TiO_2 precursor is then infiltrated into the porous layer by spin coating. The sample is then calcined at 500 °C to complete the process. Plan-view and cross-sectional SEM images of the resulting material (Fig. 1a and b, respectively) indicate that the TiO_2 layer infiltrates and coats the pores conformally and that the open pore structure is retained. The TiO_2-coated PSi film displays an average pore diameter of 66 nm, which is smaller than that of freshly etched PSi film (Fig. S2a and b). The pores are sufficiently large to accommodate the protein biomolecules used in this study, which have dimensions of 11–17 nm (Alvarez et al., 2009). The porosity and thickness of the TiO_2-coated PSi film, determined by SLIM (Segal et al., 2007), were $70 \pm 3\%$ and 5.3 ± 0.2 μm, respectively.

The X-ray spectrum of the film obtained by EDS in the electron microscope confirms that the coated PSi film contains Ti, O, and Si not only on the top of the film (Fig. S3a) but also infiltrated within the porous matrix (Fig. S3b). The FTIR spectrum of the TiO_2-coated PSi film (Fig. S4) displays an absorption band at 600–620 cm^{-1}, assigned to Ti–O vibrational modes (Tong et al., 2008) and absorption bands at 1640 cm^{-1} and 3400 cm^{-1} assigned to an –OH bending and stretching modes at the TiO_2 surface (Tong et al., 2008), respectively. After calcining at 500 °C in air, the XRD spectrum (Fig. S5) displayed peaks assigned to the (100), (200) and (211) reflections of the anatase phase of TiO_2: $2\theta = 25.2°$, 48.2°, and 55°, respectively. The average grain size of the anatase TiO_2 phase, determined from the Scherrer equation, was calculated to be 17.2 ± 0.5 nm.

The optimal spin rate, duration, and number of cycles were determined to be 2000 rpm, 10 s, and three times, respectively (Figs. S6 and S7).

3.2. Optical properties of TiO_2-coated PSi films

The spectrum of white light reflected from the TiO_2-coated film (Fig. 1c) displays optical interference fringes characteristic of thin film Fabry–Pérot interference. The optical thickness of the film can be obtained from the reflected light spectrum by Fourier transform (Fig. 1d), as described previously (Sailor, 2012). For RIFTS, the position of the peak in the Fourier transform corresponds to $2nL$, where n is the average refractive index of the porous layer of thickness L. Because the interference spectrum provides a very precise measurement of the value of the average refractive index of the porous layer, RIFTS allows for sensitive label-free optical biosensing. For example, binding of a protein to a given capture probe immobilized on the inner pore walls results in a change in average refractive index that is readily quantified using this optical method (Bonanno et al., 2010; Bonanno and Segal, 2011; Jane et al., 2009; Lin et al., 1997; Mun et al., 2010; Pacholski et al., 2005; Rendina et al., 2007; Rong and Weiss, 2009).

The sensitivity of the material used in the RIFTS analysis can be described in terms of the change in the quantity $2nL$ per unit change in average refractive index that is induced upon analyte binding (Delouise et al., 2005). For a porous optical material, sensitivity depends on a number of factors, but the four main ones are as follows: (1) resonant frequency, (2) optical quality, (3) refractive index contrast between the analyte and the analyte matrix, and (4) the total amount of analyte contained within the volume probed by the optics (Delouise et al., 2005). To quantify the absolute response of the film that could be expected for a given change in refractive index, a series of optical sensing experiments were performed using neat liquids of known refractive index. The quantity $2nL$ (optical thickness) is presented as a function of refractive index for each of a series of liquids in Fig. 2. Two sample types are compared in Fig. 2: a $PSiO_2$ sample and the TiO_2-coated PSi sample. The relationship between measured optical thickness of the film and refractive index of the organic liquid is linear for both sample types, consistent with theory and with previous reports (Delouise et al., 2005; Li and Zheng, 2008).

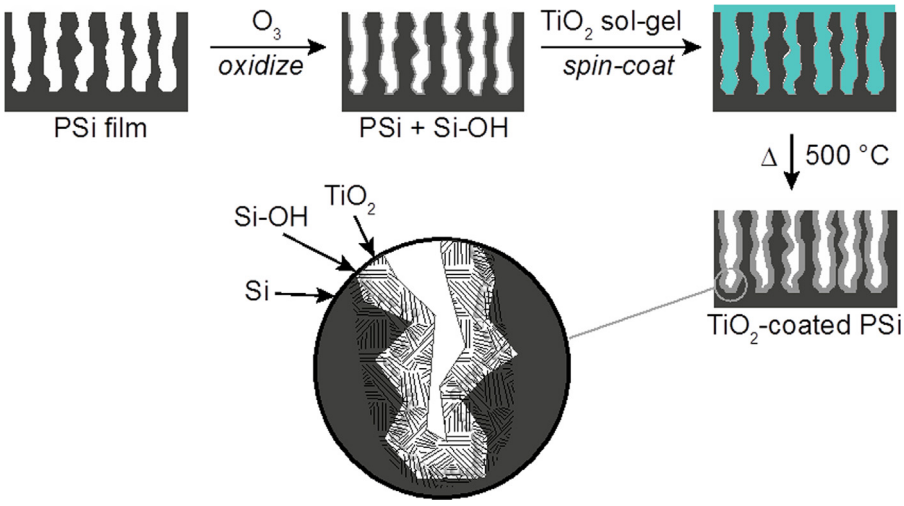

Scheme 1. The procedure scheme used to synthesize TiO_2-coated porous silicon films.

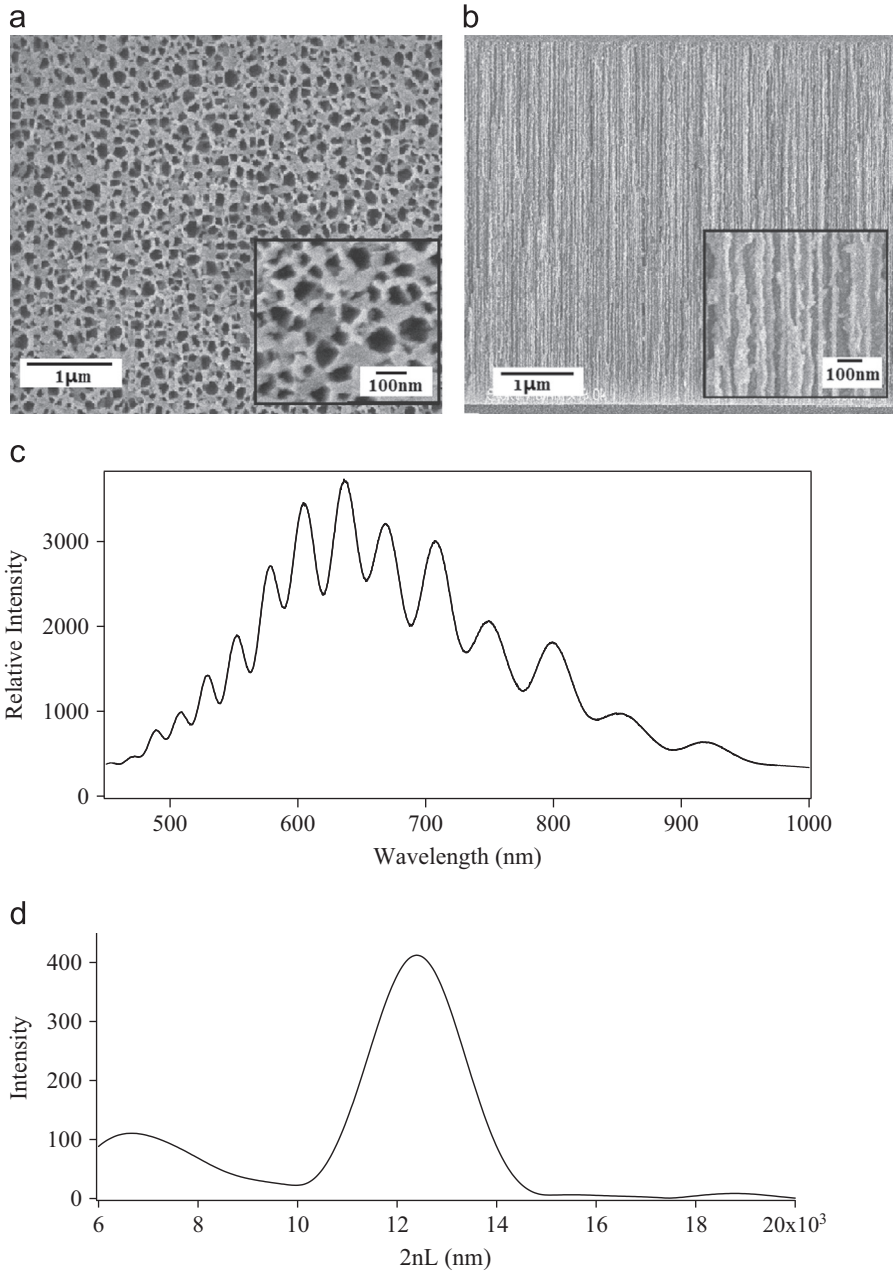

Fig. 1. Morphological and optical characteristics of TiO_2-coated PSi films. (a) Plan-view and (b) cross-sectional scanning electron microscope (SEM) images of a representative sample. The average pore diameter is 66 nm, porosity is 70%, and film thickness is 5.3 μm. (c) Reflected light spectrum from TiO_2-coated PSi film immersed in pH 7.4 PBS buffer, showing characteristic Fabry–Pérot interference fringes. (d) Fourier transform of the spectrum in (c), showing a single peak whose position along the *x*-axis corresponds to the effective optical thickness of the thin film, 2*nL*.

The sensitivity of the thermally oxidized $PSiO_2$ film and the TiO_2-coated PSi film, as measured by the slope of the curves in Fig. 2, were comparable, although the $PSiO_2$ film displayed somewhat greater sensitivity relative to the TiO_2-coated PSi film (9241 ± 217 nm/ refractive index units (RIU) vs. 8210 ± 170 nm/ RIU, respectively). These sensitivity values are comparable to the 300–8800 nm/RIU typically observed in SPR systems (Delouise et al., 2005), and somewhat larger than the 190 nm/RIU value reported for localized SPR (Haes and Van-Duyne, 2003) devices or the 450 nm/RIU value reported for TiO_2 inverse opal films (Li and Zheng, 2008).

The slightly larger slope, and thus greater sensitivity observed for the $PSiO_2$ film relative to the TiO_2-coated PSi film, is attributed to the larger porosity of the $PSiO_2$ film ($75 \pm 2\%$ vs. $70 \pm 3\%$, respectively), which is a consequence of the synthetic method used in preparation; the TiO_2 coating partially fills the porous matrix, causing a reduction in porosity. As already mentioned, successive coating steps further reduced the porosity and pore size in the films. The value of the optical thicknesses (2*nL*) measured in the optical reflectance spectrum increased with each successive coating (Figs. S6 and S7) due to the increased TiO_2 content in the film.

3.3. *Stability of the TiO_2-coated PSi film*

For label-free biosensor applications, stability of the device against zero point drift is a key parameter. The stability of the TiO_2-coated PSi film was compared to the $PSiO_2$ film by real-time

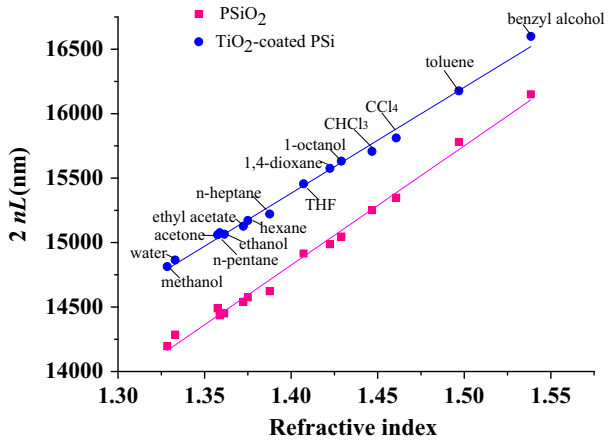

Fig. 2. Optical thickness (value of $2nL$), for a TiO_2-coated PSi (top trace, blue circles) or a $PSiO_2$ (bottom trace, red squares) film immersed in the indicated organic liquids as a function of refractive index of the liquid. Values of refractive index for the liquids are given in Supplemental Table 1. (For interpretation of the references to color in this figure legend, the reader is referred to the web version of this article.)

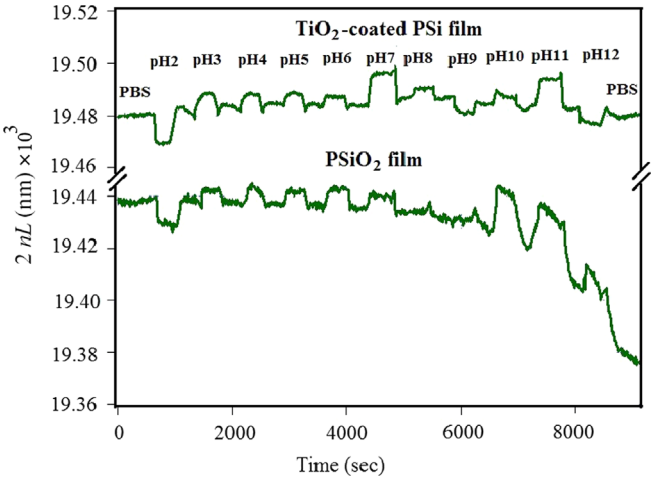

Fig. 3. Dose–response curves for TiO_2-coated PSi and $PSiO_2$ films upon exposure to buffer solutions in the range pH 2–12. Responses are quantified as optical thickness ($2nL$) vs. time during exposure to buffers of the indicated pH. The dosing cell was rinsed with pH 7.4 PBS between each buffer exposure.

monitoring of the RIFTS spectrum as buffer solutions of different pHs (2–12) were introduced to a flow cell (Fig. 3). In these experiments, each buffer has a slightly different refractive index, so each is expected to produce a slightly different equilibrium value of $2nL$ in the measurements. As seen previously (Sciacca et al., 2010; Schwartz et al., 2007a, 2007b), the $PSiO_2$ film is stable at pH ≤ 5, and the measured values of $2nL$ track the refractive index of each buffer. At pH > 7, the silicon oxide material dissolves in aqueous solution, resulting in a decrease in refractive index of the film and thus a decrease in the value of $2nL$ (Mun et al., 2010; Pacholski et al., 2006; Lees et al., 2003; Gurtner et al., 1999; Boukherroub et al., 2001;Bocking et al., 2008). By comparison, the TiO_2-coated PSi sensor was markedly more stable. The pH 7 baseline value of $2nL$ for the TiO_2-coated PSi sensor deviated by $< 0.02\%$ after exposure to a series of buffers ranging in pH from 2 to 12. The aqueous stability of the TiO_2-coated PSi sensor in these buffers was similar to the stability observed with porous TiO_2 nanotube arrays (Mun et al., 2010). However, compared with the porous TiO_2 substrate, the TiO_2-coated PSi is flexible and easy to fabricate in the design of optical nanostructures or the control of pore size.

3.4. Immunosensor experiments

The feasibility of the TiO_2-coated PSi film as an immunosensor was studied using a protein A capture probe and immunoglobulin G (IgG) antibodies. Protein A (MW $\approx$ 42 kDa) was used as a capture probe because it specifically binds to the Fc fragment of several types of antibodies. The affinity of protein A for the Fc fragment is species-dependent (Harlow and Lane, 1988a, 1988b). For example, protein A has a strong affinity for rabbit IgG, but it will not bind to chicken IgG (Harlow and Lane, 1988a, 1988b). The protein A capture probe also adsorbs strongly and non-specifically to porous SiO_2, porous TiO_2, porous Al_2O_3, and carbonized porous Si, making it a convenient molecule to test and compare the sensing properties of label-free optical biosensors (Mun et al., 2010; Alvarez et al., 2009; Schwartz et al., 2007a, 2007b; Dancil et al., 1999; Tsang et al., 2012).

Fig. 4a shows the change in optical thickness recorded from the RIFTS data when a TiO_2-coated PSi film is sequentially exposed to buffer solution 0.1 mg/mL in protein A, rabbit anti-sheep IgG, and then sheep IgG. As observed previously (Tsang et al., 2012) with the porous Si–C, porous SiO_2, and the porous TiO_2 systems, protein A binds strongly to the surface, leading to a relative change in the value of nL ($\Delta nL/nL_0\% = (nL - nL_0)/nL_0 \times 100\%$, where nL_0 is the value of nL measured immediately after introduction of the buffer solution) of $0.9 \pm 0.2\%$. This is comparable to the value observed from a $PSiO_2$ film ($1 \pm 0.2\%$) with the same porosity (Tsang et al., 2012) and somewhat larger than the value observed on porous TiO_2 nanotube arrays (0.3%; Tsang et al., 2012) and porous Al_2O_3 films (0.03%; Alvarez et al., 2009) measured in previous work. The greater signal response seen in the current experiments relative to the previous measurements is attributed to the larger surface area of the TiO_2-coated porous Si material relative to porous TiO_2 nanotube arrays (Mun et al., 2010) and porous Al_2O_3 films (Alvarez et al., 2009). The noise signal of the TiO_2-coated PSi film is lower than that of porous TiO_2 (Mun et al., 2010).

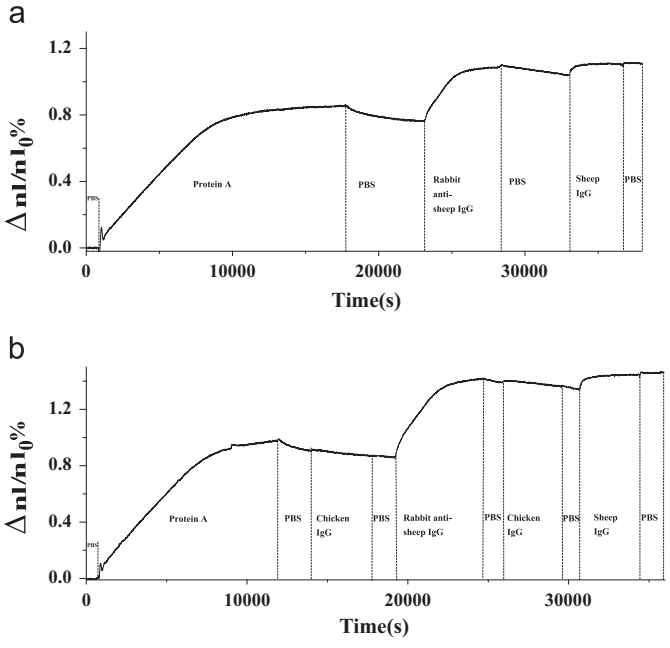

Fig. 4. Dose–response curves for TiO_2-coated PSi films upon exposure to test protein solutions at pH 7.4. Responses are quantified as relative change in optical thickness ($\Delta nL/nL_0\%$) vs. time during exposure to solutions containing the indicated protein. (a) Sequential introduction of protein A, rabbit anti-sheep IgG and sheep IgG. (b) Sequential introduction of protein A, chicken IgG, rabbit anti-sheep IgG, chicken IgG, and sheep IgG. Samples were rinsed with pH 7.4 (PBS) buffer between protein exposures as indicated. All protein solution concentrations are 0.1 mg/mL.

The protein A-treated, TiO_2-coated porous Si sample bound rabbit anti-sheep IgG, leading to an observed increase in the value of $\Delta nL/nL_0$ by $0.4 \pm 0.1\%$, indicating a binding interaction with the protein A capture probe. The relative change value is also larger than the value observed on TiO_2 nanotube arrays (0.15%) and porous Al_2O_3 films (0.16%; Tsang et al., 2012). As discussed previously, the magnitude of this increase in the value of *nL* is smaller than the value that would be predicted. Because the mass of the rabbit anti-sheep antibody is ~3.6 times greater than that of protein A, the expected increase in $\Delta nL/nL_0$ is 3.2% (Tsang et al., 2012). Such a lack of efficiency in capturing IgG has been seen in the $PSiO_2$, TiO_2, and carbonized porous Si systems previously, and it has been attributed to inaccessibility of protein A due to steric crowding effects in the relatively small pores of these materials (Tsang et al., 2012). Immunoglobulin G (IgG) is a large protein (MW ≈ 150 kDa) with an overall average diameter of 12 nm and thickness of 4 nm (Mun et al., 2010; Harlow and Lane, 1988a, 1988b; Qian et al., 2002). By comparison, the TiO_2-coated PSi film displayed an average pore diameter of 66 nm; the addition of protein A and then subsequent antibodies can be expected to constrict the pores and impede access of biomolecules.

Consistent with the steric crowding interpretation, the time required for equilibrium adsorption of protein A on the surface of the TiO_2-coated PSi film was more than 4 h longer than that was observed with TiO_2 nanotube arrays (Mun et al., 2010) or porous Al_2O_3 films (Alvarez et al., 2009). The means by which protein A adsorbs to all these porous surfaces is considered to be primarily electrostatic in nature (Chen and Sailor, 2011). Protein adsorption is considered to involve a two-step process: a rapid electrostatic attraction to the surface followed by a slower rearrangement of the adsorbed protein molecules (Moulton et al., 2004). This type of protein adsorption is influenced by pH, ionic strength, protein charge distribution, protein size, and the properties of the adsorbing surface (Delamarche et al., 1996;Topoglidis et al., 2001), and the effect on diffusion times in the nm-scale pores can be very pronounced (Chen and Sailor, 2011). The data also show that prolonged rinsing with PBS buffer generates a slow decrease in the binding signal (Fig. 4), consistent with the gradual removal of the electrostatically bound protein complex.

Finally, the sensor in the experiment shown in Fig. 4a was exposed to a secondary antibody, sheep IgG. This antibody was expected to bind to the rabbit anti-sheep antibody already bound to the sensor surface. As with the earlier protein exposures, sheep IgG displayed a lower binding affinity and equilibration rate than expected; the RIFTS response ($\Delta nL/nL_0$) was only $0.1 \pm 0.02\%$ (0.4% expected). This result can also be attributed to the steric restriction imposed by the nanometer-scale pores in the samples, which is expected to affect both the accessibility and the orientation of the capture probe. Final rinsing of the sensor with PBS buffer showed no additional change in optical thickness.

The calibration curve for sheep IgG is shown in Fig. S8. The linear detection range is from 10 to 500 μg/mL and the lower limit of detection is calculated to be 0.6 μg/mL at a signal/noise ratio of 3, which is more sensitive than the TiO_2 inverse opal (Li et al., 2008) and quartz crystal microgravimetry (Zhang et al., 2013) systems.

3.5. *Specificity of the immunosensor*

Specificity of biosensors is a critical factor, especially for label-free biodetection. Influencing factors include the specificity of the capture probe used (such as protein A, an antibody or a complementary oligonucleotide) and stability of the biosensor system (Sailor, 2007). In this work, control experiments using chicken IgG were used to establish the specificity of the protein-A-modified surface (Fig. 4b), following a previously established protocol (Alvarez et al., 2009). Introduction of chicken IgG (0.1 mg/mL) to the protein-A-modified sensor resulted in no significant change in optical thickness (quantity *nL*), indicating that chicken IgG did not bind to the protein-A-modified TiO_2-coated PSi composite film to any detectable extent. This result is consistent with the known (Harlow and Lane, 1988a, 1988b) lack of affinity of protein A for chicken IgG as discussed above. The ability of the sensor to subsequently bind rabbit IgG (Fig. 4b) as effectively as in the case where chicken IgG was not introduced (Fig. 4a) revealed that the protein A capture probe was still active. In addition, a previous report (Mun et al., 2010) indicated that IgG strongly adsorbed to the surface of porous TiO_2 and the present experiments confirmed this to also be the case with the TiO_2-coated PSi films (Fig. S9). The slight decrease in optical thickness observed in the dose–response curve (Fig. 4b) is attributed to removal of weakly bound protein A.

The specificity of the bound rabbit anti-sheep IgG was also tested. Introduction of (non-binding) chicken IgG showed no increase in the value of *nL*. Finally, sheep IgG was introduced into the sample, which generated an increase in optical thickness as discussed above for the data of Fig. 4a. A gradual decrease in optical thickness was observed throughout the binding experiments, presumably due to the slow removal of the protein A coating. A final rinse with PBS buffer showed no additional change in optical thickness. These results confirm that the prompt changes in optical thickness arise from the specific binding of the capture probes to their biomolecular binding partners.

4. Conclusions

The spin coating method introduced in this work provides a simple alternative to e-beam evaporation or magnetron sputtering (Prabakaran et al., 2007) approaches that have previously been used to place metal oxides such as TiO_2 (Betty et al., 2011; Gole et al., 2007, 2009), SnO_x, NiO, Cu_xO, Au_xO (Ozdemir and Gole, 2010) and $LiSiO_3$ (Ben-Saad et al., 2008) into PSi.

The FTIR, XRD and EDS analyses confirmed the deposition of TiO_2 layer, and the SEM and chemical stability measurements indicated that the TiO_2 layer was continuous. Label-free protein biosensor data confirmed that the pores of the resulting TiO_2–PSi composite were not blocked, although the small pores in these nanostructures led to significant effects on the diffusion and binding of proteins. The TiO_2-coated PSi film displayed a stable optical interference spectrum in aqueous solutions over the pH range 2–12. Immunosensor experiments showed that the TiO_2–PSi composite could be used as a biosensor for specific biomolecular interactions.

Acknowledgments

The authors acknowledge financial support from the U.S. National Science Foundation under Grant number NSF DMR-1210417, the National Natural Science Foundation of China under Number 31071542, Jiansu Province's Natural Science Foundation under Number BK20131398, and Jiangsu Province's Six Largest Peak Talent.

Appendix A. Supplementary material

Supplementary data associated with this article can be found in the online version at http://dx.doi.org/10.1016/j.bios.2013.12.016.

References

Alvarez, S.D., Li, C.P., Chiang, C.E., Schuller, I.K., Sailor, M.J., 2009. ACS Nano 3, 3301–3307.
Ben-Saad, K., Hamzaoui, H., Labidi, A., Bessais, B., 2008. Appl. Surf. Sci. 254, 3955–3958.
Betty, C.A., Sasikala, R., Jayakumar, O.D., Sakuntala, T., Tyagi, A.K., 2011. Prog. Photovoltaics 19, 266–274.
Bocking, T., Kilian, K.A., Gaus, K., Gooding, J.J., 2008. Adv. Funct. Mater. 18, 3827–3833.
Bolduc, O.R., Pelletier, J.N., Masson, J.-F.o., 2010. Anal. Chem. 82, 3699–3706.
Bonanno, L.M., Kwong, T.C., DeLouise, L.A., 2010. Anal. Chem. 82, 9711–9718.
Bonanno, L.M., Segal, E., 2011. Nanomedicine 6, 1755–1770.
Boukherroub, R., Wayner, D.D.M., Sproule, G.I., Lockwood, D.J., Canham, L.T., 2001. Nano Lett. 1, 713–717.
Buriak, J.M., 2002. Chem. Rev. 102, 1271–1308.
Cadarso, V.J., Fernandez-Sanchez, C., Llobera, A., Darder, M., Dominguez, C., 2008. Anal. Chem. 80, 3498–3501.
Chen, M.Y., Sailor, M.J., 2011. Anal. Chem. 83, 7186–7193.
Chen, D., Zhang, H., Li, X., Li, J.H., 2010. Anal. Chem. 82, 2253–2261.
Dancil, K.P.S., Greiner, D.P., Sailor, M.J., 1999. J. Am. Chem. Soc. 121, 7925–7930.
Delamarche, E., Sundarababu, G., Biebuyck, H., Michel, B., Gerber, C., Sigrist, H., Wolf, H., Ringsdorf, H., Xanthopoulos, N., Mathieu, H.J., 1996. Langmuir 12, 1997–2006.
DeLouise, L.A., Kou, P.M., Miller, B.L., 2005. Anal. Chem. 77, 3222–3230.
DeLouise, L.A., Miller, B.L., Haidaris, C., 2004. J. Invest. Dermatol. 122. (A136-A136).
Dupont, D., Johansson, A., Marchin, S., Rolet-Repecaud, O., Marchesseau, S., Leonil, J., 2011. J. Agric. Food Chem. 59, 8375–8384.
Gole, J.L., Lewis, S., Lee, S., 2007. Phys. Status Solidi A 204, 1417–1422.
Gole, J.L., Corno, J., Ozdemir, S., Prokes, S., Shin, H.C., 2009. Phys. Status Solidi C 6, 1773–1776.
Guan, B., Ciampi, S., Le Saux, G., Gaus, K., Reece, P.J., Gooding, J.J., 2010. Langmuir 27, 328–334.
Gurtner, C., Wun, A.W., Sailor, M., 1999. Angew. Chem. Int. Ed. 38, 1966–1968.
Haes, A.J., Van Duyne, R.P., 2003. Abstr. Pap. Am. Chem. Soc. 225. (U988-U988).
Harlow, E., Lane, D., 1988a. Antibodies: A Laboratory Manual. Cold Spring Harbor Laboratory, New York p. 726.
Harlow, E., Lane, D., 1988b. Antibodies: A Laboratory Manual. Cold Spring Harbor Laboratory, New York, pp. 310–311.
Jane, A., Dronov, R., Hodges, A., Voelcker, N.H., 2009. Trends Biotechnol. 27, 230–239.
Kang, Y., Li, X., Tu, Y.Q., Wang, Q., Agren, H., 2010. J. Phys. Chem. C 114, 14496–14502.
Lees, I.N., Lin, H.H., Canaria, C.A., Gurtner, C., Sailor, M.J., Miskelly, G.M., 2003. Langmuir 19, 9812–9817.
Li, J.L., Han, T., Wei, N.N., Du, J.Y., Zhao, X.W., 2009. Biosens. Bioelectron. 25, 773–777.
Li, J.L., Zhao, X.W., Wei, H.M., Gu, Z.Z., Lu, Z.H., 2008. Anal. Chim. Acta 625, 63–69.
Li, J.L., Zheng, T.S., 2008. Sensor Actuat. B: Chem. 131, 190–195.
Liang, F.X., Kelly, T.L., Luo, L.B., Li, H., Sailor, M.J., Li, Y.Y., 2012. Appl. Mater. Interfaces 4, 4177–4183.
Lin, V.S.Y., Motesharei, K., Dancil, K.P.S., Sailor, M.J., Ghadiri, M.R., 1997. Science 278, 840–843.
Linford, M.R., Chidsey, C.E.D., 1993. J. Am. Chem. Soc. 115, 12631–12632.
Meskini, O., Abdelghani, A., Tlili, A., Mgaieth, R., Jaffrezic-Renault, N., Martelet, C., 2007. Talanta 71, 1430–1433.
Moulton, S.E., Barisci, J.N., Bath, A., Stella, R., Wallace, G.G., 2004. Langmuir 21, 316–322.
Mun, K.-S., Alvarez, S.D., Choi, W.-Y., Sailor, M.J., 2010. ACS Nano 4, 2070–2076.
Orosco, M.M., Pacholski, C., Sailor, M.J., 2009. Nat. Nanotechnol. 4, 255–258.
Ouyang, H., Christophersen, M., Viard, R., Miller, B.L., Fauchet, P.M., 2005. Adv. Funct. Mater. 15, 1851–1859.
Ozdemir, S., Gole, J.L., 2010. Sensor Actuat. B: Chem. 151, 274–280.
Pacholski, C., Sartor, M., Sailor, M.J., Cunin, F., Miskelly, G.M., 2005. J. Am. Chem. Soc. 127, 11636–11645.
Pacholski, C., Yu, C., Miskelly, G.M., Godin, D., Sailor, M.J., 2006. J. Am. Chem. Soc. 128, 4250–4252.
Prabakaran, R., Monteiro, T., Peres, M., Viana, A.S., Da Cunha, A.F., Aguas, H., Goncalves, A., Fortunato, E., Martins, R., Ferreira, I., 2007. Thin Solid Films 515, 8664–8669.
Qian, W.P., Gu, Z.Z., Fujishima, A., Sato, O., 2002. Langmuir 18, 4526–4529.
Rendina, I., Rea, I., Rotiroti, L., De Stefano, L., 2007. Physica E 38, 188–192.
Rong, G., Weiss, S.M., 2009. Phys. Status Solidi A 206, 1365–1368.
Sailor, M.J., 2007. ACS Nano 1, 248–252.
Sailor, M.J., 2012. Porous Silicon in Practice: Preparation, Characterization and Applications. Wiley-VCH, Weinheim, Germany.
Schwartz, M.P., Alvarez, S.D., Sailor, M.J., 2007a. Anal. Chem. 79, 327–334.
Schwartz, M.P., Yu, C., Alvarez, S.D., Migliori, B., Godin, D., Chao, L., Sailor, M.J., 2007b. Phys. Status Solidi A 204, 1444–1448.
Sciacca, B., Alvarez, S.D., Geobaldo, F., Sailor, M.J., 2010. Dalton Trans. 39, 10847–10853.
Segal, E., Perelman, L.A., Cunin, F., Di Renzo, F., Devoisselle, J.M., Li, Y.Y., Sailor, M.J., 2007. Adv. Funct. Mater. 17, 1153–1162.
Song, Y.Y., Schmuki, P., 2010. Electrochem. Commun. 12, 579–582.
Tong, T.Z., Zhang, J.L., Tian, B.Z., Chen, F., He, D.N., 2008. Mater. Lett. 62, 2970–2972.
Topoglidis, E., Campbell, C.J., Cass, A.E.G., Durrant, J.R., 2001. Langmuir 17, 7899–7906.
Tsang, C.K., Kelly, T.L., Sailor, M.J., Li, Y.Y., 2012. ACS Nano 6, 10546–10554.
Van Noort, D., Welin-Klintstrom, S., Arwin, H., Zangooie, S., Lundstrom, I., Mandenius, C.F., 1998. Biosens. Bioelectron. 13, 439–449.
Wei, N.N., Han, T., Deng, G.Z., Li, J.L., Du, J.Y., 2011. Thin Solid Films 519, 2409–2414.
Zhang, Y.X., Islam, N., Carbonell, R.G., Rojas, O.J., 2013. Anal. Chem. 85, 1106–1113.